Date of publication xxxx 00, 0000, date of current version xxxx 00, 0000.

Digital Object Identifier 10.1109/ACCESS.2017.DOI

Sample-Efficient Spatio-Spectral Whitespace Detection Using Least Matching Pursuit

EMRE GÖNÜLTAŞ[1] (Student Member, IEEE), SWETA SONI[2] (Student Member, IEEE), ALYSSA B. APSEL[2] (Fellow, IEEE), and CHRISTOPH STUDER[3] (Senior Member, IEEE)

[1]Ericsson, Austin, TX 78704 USA
[2]School of Electrical and Computer Engineering, Cornell University, Ithaca, NY 14853, USA
[3]Department of Information Technology and Electrical Engineering, ETH Zürich, Zürich, Switzerland

Corresponding author: Emre Gönültaş (e-mail: eg566@cornell.edu).

EG was with the School of Electrical and Computer Engineering, Cornell University, Ithaca, NY 14853 USA, and is now with Ericsson, Austin, TX 78704, USA. The work of EG, SS, ABA, and CS was supported by the US National Science Foundation (NSF) under grant ECCS-1824379. The work of EG and CS was also supported in part by the US NSF under grants CNS-1717559 and CNS-1955997.

ABSTRACT

Multi-antenna wireless communication improves spectral efficiency by reusing frequencies at different locations in space using beamforming and spatial multiplexing. In the past, research has extensively focused on dynamically reusing unused frequency bands to optimize spectrum usage, but methods that identify unused resources in space appear to be unexplored. In this paper, we propose a sample-efficient whitespace detection pipeline for multi-antenna radio-frequency (RF) transceivers that detects unused resources in both frequency and space. Our spatio-spectral whitespace detection pipeline relies on multi-antenna nonuniform wavelet sampling, which identifies unused frequencies in space at sub-Nyquist sampling rates. We demonstrate the efficacy of our approach via system simulations and show that reliable spatio-spectral whitespace detection is possible with 16× lower sampling rates than methods relying on Nyquist sampling.

INDEX TERMS Coherence, compressive sensing (CS), least matching pursuit (LMP), multi-antenna communication, nonuniform wavelet sampling (NUWS), spatio-spectral sensing, whitespace detection.

I. INTRODUCTION

The trend towards global digitalization requires ubiquitous wireless connectivity and most wireless services rely on mobile devices with limited battery capacity. Mainly driven by the Internet of Things (IoT), the number of connected devices is predicted to grow to 13.1 B by 2023 [1]. Such excessively large numbers of wireless devices combined with the ever-growing need for higher data-rates will inevitably cause congestion in the radio-frequency (RF) spectrum and lead to significant challenges in making efficient use of the spectrum. Because of the limitations in RF spectrum allocation and limited battery capacity of IoT devices, it is critical to deploy energy-efficient sensing methods that identify unused RF channels with the goal of opportunistically reusing the available resources among devices at both the infrastructure base station (BS) and the user equipment (UE) sides.

Massive multi-user multiple-input multiple-output (MU-MIMO) [2]–[4], exploits the concept of reusing the spectrum in space by deploying hundreds of BS antenna elements while simultaneously communicating with tens of UEs. Such large antenna arrays enable extremely fine-grained beamforming at the BS-side, which can be used to precisely focus useful energy towards the UEs, resulting in energy-efficient communication [5]. Although the impact of these technologies is evident, only little attention has been given to identifying unused resources in *space*.

A. SPATIO-SPATIAL WHITESPACE DETECTION

Identifying whitespaces in both the frequency and spatial domains enable one to reallocate services from one frequency to another while keeping spatial occupancy (e.g., angle-of-arrival in line-of-sight scenarios or spatio-spectral signature in rich scattering environments) in mind using a new paradigm we call *spatio-spectral defragmentation*. The operating principle of this idea is illustrated in Figure 1, which shows a massive MU-MIMO BS serving three single-antenna UEs under line-of-sight (LoS) channel conditions. The top-right part of Figure 1 illustrates traditional whitespace detection,

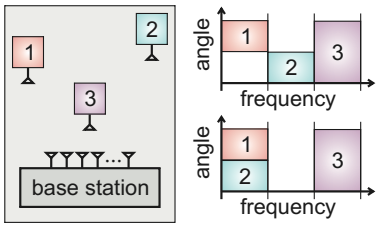

FIGURE 1. Principle of spatio-spectral whitespace detection and defragmentation: (left) multi-antenna BS serving three UEs; (top right) all three frequency bands appear occupied by ignoring the angular (spatial) domain; (bottom right) spatio-spectral whitespace detection and spectrum defragmentation releases bandwidth that can be used for communication.

which would indicate that all of the available frequencies are occupied. However, by taking into account the spatial dimension (we consider the incident angle in this LoS case), we can relocate UE 2 to use the frequency that is also used by UE 1 without causing interference—this is possible because the two UEs can be separated in space by means of beamforming. Since this spectrum relocation liberates the middle frequency band, there is now a new unused frequency band that could be used for transmission, even by single antenna UEs. The advantages of spatio-spectral defragmentation are manifold: (i) reduced interference among UEs which results in improved signal-to-noise ratio (SNR); (ii) separation of UEs in frequency and space, which mitigates the need for time-division duplexing, hence, reducing latency; (iii) enabling more UEs to use the spectrum which increases the total number of devices that can share the available spectrum; (iv) releasing adjacent frequencies for transmitters or services that require larger contiguous bandwidth.

B. COMPRESSIVE SPECTRUM SENSING

Extracting frequency and spatial occupancy information can be implemented in the following ways: (i) Frequency scanning [6], [7], which relies on Nyquist sampling, or (ii) compressive sensing (CS), which samples analog signals below the Nyquist rate [8], [9]. While frequency scanning enables high sensitivity in distinguishing weak RF channels from noise, it is slow and sample inefficient [10]. In contrast, CS has the potential to reduce signal acquisition times and improve sample efficiency with the assumption of spectral sparsity, i.e., the concept that only a few RF channels are occupied at a given time instant. CS has been proposed in the past for the detection of strong transmitters in the RF spectrum [11]–[16] and for direction-of-arrival detection [17]. For such CS-based applications, circuit-level implementations have been described in the literature [18]–[22]. However, CS is sensitive to noise [23], which limits conventional CS-based wideband spectrum sensing algorithms to detecting only strong signals, i.e., occupied RF channels [13], [18], [24]. Furthermore, identifying used RF channels via CS typically requires complex signal recovery algorithms [25]–[28], which often annihilates the advantages of sampling efficiency [18].

With the exceptions of [29], [30], to the best of our knowledge, no work describes whitespace detection methods using

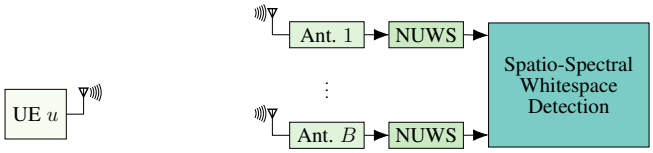

FIGURE 2. Overview of the proposed spatio-spectral whitespace detection framework. NUWS acquires compressed measurements at each receive antenna in a uniform linear array (ULA). A spatio-spectral whitespace detection algorithm then identifies whitespaces in both space and frequency.

CS measurements. Reference [29] proposed zero detection group thresholding (ZD-GroTH), which is a general algorithm to detect unused components in sparse signals. Reference [30] recently proposed least matching pursuit (LMP) which improves upon ZF-GroTH and enables one to identify *unused* channels in the RF spectrum using nonuniform wavelet sampling (NUWS), which avoids many of the drawbacks of traditional CS-based approaches [24]. However, the CS-based whitespace detection framework in [30] was designed for single-antenna systems only, which prevents its use for spatio-spectral whitespace detection and defragmentation.

C. CONTRIBUTIONS

In this paper, we develop a novel framework that detects spatio-spectral whitespace using multi-antenna NUWS [24]. Our framework extends the recently-introduced LMP algorithm for single-antenna systems in [30] to multi-antenna NUWS measurements in order to identify an unused spatio-spectral resource block. We provide new theory on proper system modeling for multi-antenna NUWS receivers and propose design criteria for multi-antenna NUWS sensing matrices. We show that properly-designed NUWS-based sensing matrices yield low overall block mutual coherence, which results in better whitespace detection performance than simply applying the methods from [30] to multi-antenna systems. In order to demonstrate the efficacy of our framework, we simulate a spatio-spectral whitespace detection task with a realistic NUWS-based multi-antenna RF system model, and we compare our approach to Nyquist sampling and the method from [30].

D. NOTATION

Uppercase boldface letters denote matrices; lowercase boldface letters denote column vectors. For a matrix $\mathbf{A}$, we denote its transpose by $\mathbf{A}^T$, its Hermitian transpose by $\mathbf{A}^H$, and complex-conjugate by $\mathbf{A}^*$. We write $[\mathbf{A}]_i$ to refer to the ith block (or submatrix), which is a collection of adjacent columns in $\mathbf{A}$. The entry in the kth row and qth column of matrix $\mathbf{A}$ is denoted by $A_{k,q}$. The spectral norm of $\mathbf{A}$ is $\|\mathbf{A}\|_2 = \sigma_{\max}$, where $\sigma_{\max}$ is the largest singular value. The matrix $\mathbf{F}_N$ is the $N \times N$ unitary discrete Fourier transform (DFT) matrix. The matrix $\mathbf{I}_N$ is the $N \times N$ identity matrix. The ℓ_2-norm of a vector $\mathbf{a}$ is $\|\mathbf{a}\|_2$. The Kronecker-product is $\otimes$ and $\mathrm{vec}(\mathbf{A})$ vectorizes the matrix $\mathbf{A}$. The real and imaginary parts of a vector $\mathbf{a}$ are denoted by $\Re(\mathbf{a})$ and $\Im(\mathbf{a})$, respectively.

II. SYSTEM MODEL

We now develop a model for the system in Figure 2. We consider a single-antenna UE with index u transmitting data to a B-antenna receiver. The receiver captures the transmitted RF signal at a uniform linear array (ULA) using NUWS. A spatio-spectral whitespace detection algorithm then identifies unused resources in both space and frequency.

A. SINGLE-INPUT MULTIPLE-OUTPUT BASEBAND MODEL

Let $v_u(t)$ be the complex-valued time-domain baseband message signal with a bandwith of Z Hz. Assume that the uth UE is transmitting this signal by modulating it with a carrier frequency f_u centered around f_c as $f_u = f_c + f_q$, where f_c is the center frequency of the band of interest and $f_q \in \{-ZC/2, -ZC/2 + Z, \ldots, ZC/2 - Z\}$ is the subchannel frequency that can be chosen among C uniformly-spaced subchannels in that frequency band which has a total bandwidth of ZC Hz. The modulated transmit RF signal at carrier frequency f_u of the uth user is given by [31]

$$\overline{v}_u(t) = \Re\{v_u(t)e^{j2\pi f_u t}\}. \tag{1}$$

We consider a block-fading multi-path scenario and a multi-antenna receiver with a B-antenna ULA. The (noise-free) received RF signal at BS antenna b can be modeled as

$$\overline{r}_{b,u}(t) = \sum_{\ell=1}^{L} a_{u,\ell}\overline{v}_u(t - \tau_{b,u,\ell}). \tag{2}$$

Here, L is the total number of propagation paths (including a possible line-of-sight path and reflections), $a_{u,\ell}$ is the (real-valued) attenuation between UE u and the receiver associated with path ℓ, where we assume that the attenuation is equal for all B receive antennas, and $\tau_{b,u,\ell}$ is the time-of-flight of the ℓth path between the UE u and BS antenna b. With (1), the received RF signal at antenna b can be written as

$$\overline{r}_{b,u}(t) = \sum_{\ell=1}^{L} a_{u,\ell}\Re\left\{v_u(t - \tau_{b,u,\ell})e^{j2\pi f_u(t-\tau_{b,u,\ell})}\right\} \tag{3}$$

$$= \Re\left\{\sum_{\ell=1}^{L} a_{u,\ell}e^{-j2\pi f_u\tau_{b,u,\ell}}v_u(t - \tau_{b,u,\ell})e^{j2\pi f_u t}\right\}. \tag{4}$$

At the BS, we perform down-conversion of the received signal in (4) by mixing it with a complex sinusoid at the band's center frequency f_c and low-pass filtering the result to obtain the following complex-valued baseband signal:

$$r_{b,u}(t) = \sum_{\ell=1}^{L} a_{u,\ell}e^{-j2\pi f_u\tau_{b,u,\ell}}v_u(t - \tau_{b,u,\ell})e^{j2\pi f_q t}. \tag{5}$$

We assume that the ULA at the receiver has an antenna spacing of Δ_a and the distance between the transmitter (and scatterers) and the receiver is much larger than the size of the antenna array. With these assumptions, we can approximate the time-of-flight using the plane-wave approximation as [32]

$$\tau_{b,u,\ell} \approx \frac{d_{u,\ell}}{c} + (b-1)\frac{\Delta_a}{c}\cos(\phi_{u,\ell}), \tag{6}$$

where $d_{u,\ell}$ is the distance between scatterer (or UE) ℓ and the first BS antenna, c is the speed of electromagnetic waves, and $\phi_{u,\ell}$ is the incident angle to the ULA of the ℓth transmission path. We can now model the joint effect of the attenuation and delay across each antenna element $\alpha_{b,u,\ell}$ in (5) using the following approximation

$$\alpha_{b,u,\ell} = a_{u,\ell}e^{-j2\pi f_u\tau_{b,u,\ell}} \tag{7}$$

$$\approx \tilde{a}_{u,\ell}e^{-j2\pi f_u(b-1)\frac{\Delta_a}{c}\cos(\phi_{u,\ell})}, \tag{8}$$

where we have absorbed the $d_{u,\ell}$-dependent term into the complex-valued attenuation $\tilde{a}_{u,\ell}$. We also assume that the bandwidth Z of the message signal $v_u(t)$ is much smaller than the inverse propagation delay across the BS antenna array, which leads to the approximation [33]

$$v_u(t - \tau_{b,u,\ell}) \approx v_u\left(t - \frac{d_{u,\ell}}{c}\right) = v_{u,\ell}(t), \tag{9}$$

removing any antenna-index-dependence from the received (and delayed) message signal $v_{u,\ell}(t)$. By combining (6) and (9), we obtain in-phase and quadrature samples of (5) at a sampling period T_s, which leads to the following model for the complex-valued discrete-time receive baseband signal:

$$r_b[n] = \sum_{\ell=1}^{L} \alpha_{b,u,\ell}v_{u,\ell}(nT_s)e^{j2\pi f_q nT_s}. \tag{10}$$

B. BLOCK-SPARSE MULTI-USER BASEBAND MODEL

We now model the discrete-time receive signal for all B antennas. We define the array-response (row) vector

$$\mathbf{k}_{u,\ell}^H \triangleq [\alpha_{1,u,\ell},\ \alpha_{2,u,\ell},\ \ldots,\ \alpha_{B,u,\ell}], \tag{11}$$

which contains all antenna-dependent terms from (10). We also define the message signal (column) vector

$$\mathbf{v}_{u,\ell} \triangleq [v_{u,\ell}(0), \ldots, v_{u,\ell}\left((N-1)T_s\right)e^{j2\pi f_q T_s(N-1)}]^T, \tag{12}$$

which contains N samples of the received (and delayed) message signal. With both of these definitions, we can write the N received samples at all B antennas in compact matrix form as follows:

$$\mathbf{X}_u = \sum_{\ell=1}^{L} \mathbf{v}_{u,\ell}\mathbf{k}_{u,\ell}^H. \tag{13}$$

We now assume the presence of U UEs at different locations that transmit data simultaneously and in the same frequency band but possibly occupying different subchannels. This situation can be modeled as

$$\mathbf{X} = \sum_{u=1}^{U} \mathbf{X}_u + \mathbf{N}, \tag{14}$$

where we also model thermal noise $\mathbf{N} \in \mathbb{C}^{N\times B}$.

In practice, wireless transmitters typically only occupy a few frequencies and spatial resources at a given time instant, which results in sparsity in both the frequency and spatial domains [31]. Since phase rotations in the sample domain

correspond to frequency shifts in the DFT domain, we can transform the samples for each BS antenna into the DFT domain as $\hat{\mathbf{X}} = \mathbf{F}_N \mathbf{X}$, which contains the frequency response of each antenna in its columns. By taking another DFT across the antenna array, we transform the antenna domain into the so-called beamspace domain [34]

$$\mathbf{S} = \hat{\mathbf{X}} \mathbf{F}_B^T = \mathbf{F}_N \mathbf{X} \mathbf{F}_B^T, \tag{15}$$

which represents the incident angles for each frequency in its rows. The matrix $\mathbf{S} \in \mathbb{C}^{N \times B}$ compactly captures the spatio-spectral structure of the received signal: The columns indicate (active) beams (i.e., angles) and the rows indicate (active) frequencies. If only a few UEs are present and the number of propagation paths L per UE is small (which is the case in many outdoor sub-6-GHz and millimeter-wave channels), then the matrix $\mathbf{S}$ will be *sparse*, i.e., only a few entries will have large magnitudes. Here, taking the DFT over the time domain reveals the sparse frequency structure; taking the DFT over the antenna (e.g., a uniform linear array) reveals the sparse structure in the beamspace (angular) domain [34].

In what follows, we assume that the vectorized signal $\mathbf{s} = \mathrm{vec}(\mathbf{S})$ in (15) contains K spectral blocks for each beam with $\mathbf{s}_i \in \mathbb{C}^{N_i}$ each of dimension N_i, where $i = 1, \ldots, K$, $\sum_{i=1}^{K} N_i = N$, and $\mathbf{s} = [\mathbf{s}_1^H, \ldots, \mathbf{s}_{BK}^H]^H$; and, thanks to sparsity, J of these blocks have large magnitudes, i.e., the vector $\mathbf{s}$ is modeled as a J-block-sparse signal [35]. This block sparsity is key in the whitespace detection pipeline we develop in the remainder of the paper.

C. COMPRESSIVE SENSING (CS) BASICS

Our goal is to detect unused resources in frequency and (beam)space represented while avoiding Nyquist sampling. To this end, we exploit the block sparsity of $\mathbf{s} = \mathrm{vec}(\mathbf{S})$ using CS [8] and acquire linear measurements as follows:

$$\mathbf{y} = \mathbf{\Theta} \mathbf{s}. \tag{16}$$

Here, $\mathbf{y} \in \mathbb{C}^{BM}$ contains the compressed measurements with $BM \ll BN$, and $\mathbf{\Theta} \in \mathbb{C}^{BM \times BN}$ is the effective sensing matrix which combines the joint effect of the sensing matrix and the sparsifying transform. Here, the ratio $\eta \triangleq \frac{BM}{BN}$ is the *subsampling rate*. To reveal the block-sparse structure, we can write an equivalent system model $\mathbf{y} = \sum_{i=1}^{K} [\mathbf{\Theta}]_i \mathbf{s}_i$, where $[\mathbf{\Theta}]_i$ is the ith block of the effective sensing matrix $\mathbf{\Theta} = [[\mathbf{\Theta}]_1, \ldots, [\mathbf{\Theta}]_K]$ with $[\mathbf{\Theta}]_i \in \mathbb{C}^{BM \times N_i}$.

CS acquires measurements by computing inner products in the time domain via $\mathbf{y} = \mathbf{Q}\mathbf{x}$, where $\mathbf{x} = \mathrm{vec}(\mathbf{X})$ is the vectorized time domain signal in (14) and $\mathbf{Q} \in \mathbb{C}^{BM \times BN}$ is the sensing matrix. The effective sensing matrix is $\mathbf{\Theta} = \mathbf{Q}\mathbf{\Psi}^{-1}$, where $\mathbf{\Psi}^{-1} \in \mathbb{C}^{BN \times BN}$ is the inverse sparsifying transform with $\mathbf{x} = \mathbf{\Psi}^{-1}\mathbf{s}$. For the multi-antenna RF signal model in (15), we have that $\mathbf{\Psi}^{-1} = \mathbf{F}_B^H \otimes \mathbf{F}_N^H$.

D. NONUNIFORM WAVELET SAMPLING (NUWS)

As shown in Figure 2, we use NUWS [24] to acquire CS measurements at each antenna. NUWS efficiently samples analog signals by taking inner products between the analog signal and wavelets that can be generated efficiently in hardware [36]. For antenna b, the NUWS measurement process can be modeled as $\mathbf{y}_b = \mathbf{W}_b \mathbf{x}_b$, where $\mathbf{y}_b \in \mathbb{C}^M$ contains the M wavelet coefficients with $M \ll N$, $\mathbf{W}_b \in \mathbb{C}^{M \times N}$ is the NUWS sensing matrix containing wavelets $\mathbf{w}_m \in \mathbb{C}^N$, $m = 1, \ldots, M$, on each row, and $\mathbf{x}_b \in \mathbb{C}^N$ is the received signal at the bth antenna (the bth column of $\mathbf{X}$). Each wavelet $\mathbf{w}_m(\delta_m, f_m, \sigma_m)$ can be tuned in time (δ), frequency (f), and pulse width (σ). By carefully selecting these parameters for all M wavelets, one can effectively subsample the signal $\mathbf{x}_b$ while preserving the information of interest [24], [30].

We can write the NUWS process for all B antennas as follows. Let $\mathbf{Y} \in \mathbb{C}^{M \times B}$ be a matrix containing NUWS measurements for the B antennas in its columns as $\mathbf{Y} = [\mathbf{y}_1, \mathbf{y}_2, \ldots, \mathbf{y}_B]$. By vectorizing this matrix $\tilde{\mathbf{y}} = \mathrm{vec}(\mathbf{Y})$, the NUWS measurement process can be written as follows:

$$\tilde{\mathbf{y}} = \tilde{\mathbf{Q}}\,\mathbf{x}. \tag{17}$$

Here, the block-diagonal multi-antenna NUWS sensing matrix $\tilde{\mathbf{Q}} \in \mathbb{C}^{BM \times BN}$ is defined as $\tilde{\mathbf{Q}} \triangleq \mathrm{diag}(\mathbf{W}_1, \mathbf{W}_2, \ldots, \mathbf{W}_B)$. The effective multi-antenna NUWS sensing matrix in (16) is $\mathbf{\Theta} = \tilde{\mathbf{Q}}\mathbf{\Psi}^{-1}$, which combines the effect of NUWS $\tilde{\mathbf{Q}}$ and the inverse sparsifying transform $\mathbf{\Psi}^{-1}$ defined in section II-C.

III. SPATIO-SPECTRAL WHITESPACE DETECTION

We now show how to detect unused resources in both space and frequency from multi-antenna NUWS measurements. We then propose a method to design suitable wavelet dictionaries.

A. LEAST MATCHING PURSUIT (LMP)

In order to identify a spatio-spectral whitespace using multi-antenna NUWS measurements, we use LMP introduced in [30] for single-antenna receivers. LMP resembles block orthogonal matching pursuit (BOMP) [35] and starts with an initial residual $\mathbf{r}^0 = \tilde{\mathbf{y}}$. In each LMP iteration $t = 1, \ldots, P$, one first correlates each block $[\mathbf{\Theta}]_i$ with the residual $\mathbf{r}^t$ as

$$\lambda_i^{t+1} = \|[\mathbf{\Theta}]_i^H \mathbf{r}^t\|_2, \quad i = 1, \ldots, K, \tag{18}$$

followed by identifying the most-correlating block

$$c^{t+1} = \underset{i=1,\ldots,K}{\arg\max}\, \lambda_i^{t+1}. \tag{19}$$

LMP then augments the support set $\Omega^{t+1} = \Omega^t \cup c^{t+1}$, followed by computing an estimate of the non-zero blocks via $\hat{\mathbf{s}}_{\Omega^{t+1}} = \mathbf{\Theta}_{\Omega^{t+1}}^{\dagger} \tilde{\mathbf{y}}$, where $\mathbf{\Theta}_{\Omega^{t+1}}$ is a concatenation of the blocks indexed by Ω^{t+1}. LMP then computes a new residual according to $\mathbf{r}^{t+1} = \tilde{\mathbf{y}} - \mathbf{\Theta}_{\Omega^{t+1}} \hat{\mathbf{s}}_{\Omega^{t+1}}$. After P iterations, LMP uses the collected coefficients in (18) to identify the least-correlating block index $\hat{f}$ according to

$$\hat{f} = \underset{i \in \{1,2,\ldots,K\} \setminus \Omega^{P+1}}{\arg\min} \sum_{t=1}^{P} \lambda_i^{t+1}. \tag{20}$$

To assess the complexity of LMP, we provide a complexity analysis in Table 1 by counting the number of real-valued

TABLE 1. Computational complexity of frequency scanning and LMP.

Algorithm	Complexity
Frequency scanning	$BN(\log_2 B + \log_2 N) + 2BN$
LMP	$4BN(\eta BN)^2 + 2BN + 2(BN/K)^3 + 6\eta BN(BN/K)^2$ $-2\eta(BN)^2/K + 4BN/K(\eta BN)^2 + 4\eta BN(BN/K)^2$

multiplications required for (i) traditional frequency scanning using a fast Fourier transform (FFT) and (ii) LMP with $P = 1$ as a function of the subsampling ratio defined as $\eta = \frac{BM}{BN}$. Frequency scanning takes in a $B \times N$ dimensional antenna-domain matrix $\mathbf{X}$ and applies 2D-FFT which has a complexity of $BN(\log_2 B + \log_2 N)$ followed by calculating the energy of each block $\mathbf{s}_i \in \mathbb{C}^{N_i}$ that requires $2BN$ real-valued multiplications. Our approach requires $4BN(\eta BN)^2 + 2BN$ real-valued multiplications for calculating the correlation in (18), $2(BN/K)^3 + 6\eta BN(BN/K)^2 - 2\eta(BN)^2/K) + 4BN/K(\eta BN)^2$ real-valued multiplications for estimating the non-zero blocks $\hat{\mathbf{s}}_{\Omega^{t+1}}$, and $4\eta BN(BN/K)^2$ real-valued multiplications for calculating the residual $\mathbf{r}^{t+1}$. We note that frequency scanning is typically less complex than LMP. Nonetheless, in many practical applications, sampling, storage, and data transmission are typically the limiting factors as whitespace detection can be calculated in the cloud (where computational resources are abundant and spectral defragmentation would be carried out). In applications that require on-device whitespace detection from CS-measurement, more efficient algorithms than LMP would need to be developed.

B. BLOCK COHERENCE ANALYSIS OF EFFECTIVE SENSING MATRIX

As shown in [30] for the single-antenna case, the performance of LMP critically depends on the effective sensing matrix. Concretely, one of the determining performance factors is the block coherence [35], which we define as follows.

Definition 1. *The block coherence of the effective sensing matrix $\mathbf{\Theta}$ is defined as follows:*

$$\mu_{\mathbf{\Theta}} \triangleq \max_{i \neq i'} \left\| [\mathbf{\Theta}]_i^H [\mathbf{\Theta}]_{i'} \right\|_2 . \tag{21}$$

We note that the block coherence is a standard tool to characterize the performance of compressive sensing algorithms that recover strong components of block-sparse signals [35]. Concretely, if the block coherence is sufficiently small, then a block sparse signal $\mathbf{x}$ can be recovered by from noiseless compressed measurements. The paper [30] has shown recently that the block coherence is also relevant to provide conditions when whitespace detection is possible—not just to detect strong signal components. We next show that the block coherence in (21) is also relevant for detecting unused resources in both the frequency and spatial domains. Concretely, we now show that it matters whether one uses different NUWS matrices $\mathbf{W}_b$, $b = 1, \ldots, B$, at each of the B antenna elements or whether one uses the same set of wavelets at each antenna, i.e., $\mathbf{W}_1 = \mathbf{W}_b$, $b = 1, \ldots, B$. For simplicity, we assume (A1) equally sized blocks $N_i = N/K$ and (A2) unitary blocks in the NUWS matrices $[\mathbf{W}_b]_k^H [\mathbf{W}_b]_k = \mathbf{I}_{N_i}$, $b = 1, \ldots, B$, and $k = 1, \ldots, K$, where k is the block index.

We first analyze the block coherence of the case in which different NUWS sensing matrices are used at each antenna. We have the following result; the proof is given in Appendix A.

Proposition 1. *Using (A1) and (A2), the block coherence $\mu_{\mathbf{\Theta}}$ of the effective sensing matrix $\mathbf{\Theta}$ satisfies*

$$\mu_{\mathbf{\Theta}} \leq \frac{1}{B} \sum_{b=1}^{B} \mu_{\hat{\mathbf{W}}_b}, \tag{22}$$

where $\mu_{\hat{\mathbf{W}}_b}$ is the block coherence of the frequency-domain NUWS sensing matrix $\hat{\mathbf{W}}_b = \mathbf{W}_b \mathbf{F}_N^H$ at antenna b.

This result shows that using different NUWS matrices per receive antenna has the potential to yield lower block coherence than the average of the individual block coherences of the frequency-domain NUWS matrices.

We now analyze the case in which the same NUWS sensing matrix $\mathbf{W}_1$ is used at each antenna. We have the following result; the proof is given in Appendix B.

Proposition 2. *Using (A1) and (A2), the block coherence $\mu_{\mathbf{\Theta}}$ of the effective sensing matrix $\mathbf{\Theta}$ satisfies*

$$\mu_{\mathbf{\Theta}} = \mu_{\hat{\mathbf{W}}_1}, \tag{23}$$

where $\mu_{\hat{\mathbf{W}}_1}$ is the block coherence of the frequency-domain NUWS matrix $\hat{\mathbf{W}}_1 = \mathbf{W}_1 \mathbf{F}_N^H$ at antenna 1.

This result shows that using the same NUWS matrix at each receive antenna renders the block coherence of $\mathbf{\Theta}$ to be the same as that of the frequency-domain NUWS matrix $\hat{\mathbf{W}}_1$. Consequently, the use of different NUWS matrices at each receive antenna has the potential to reduce the block coherence and, hence, improve the performance of LMP for spatio-spectral whitespace detection. We will confirm this observation via system simulations in section IV on the next page.

C. DESIGN OF EFFECTIVE SENSING MATRICES

We now describe the design of sensing matrices for spatio-spectral whitespace detection that have small block coherence. We start by generating an overcomplete NUWS *base dictionary* $\underline{\mathbf{W}} \in \mathbb{C}^{D \times N}$ consisting of $D \gg M$ different wavelets. As in the single-antenna case [30], [37], we focus on wavelet sequences with elements taken from the set $\{+1, 0, -1\}$, which has the advantage of enabling simple analog circuitry to generate the wavelet sequences. From this base dictionary, we generate an overcomplete block-diagonal base dictionary for the multi-antenna case as $\underline{\mathbf{Q}} = \mathbf{I}_B \otimes \mathbf{W}_D$. We then use a greedy, wrapper-based algorithm to select a subset of BM wavelet sequences with small block coherence from this base dictionary. To this end, we start with an empty set of wavelet sequences. For each sequence in the overcomplete dictionary, we utilize the following self-orthogonalizing version of the block coherence defined as [30]

$$\bar{\mu}_{\mathbf{\Theta}^v} \triangleq \max_{i \neq i'} \left\| ([\mathbf{\Theta}^v]_i^H [\mathbf{\Theta}^v]_i)^{-0.5} [\mathbf{\Theta}^v]_i^H [\mathbf{\Theta}^v]_{i'} \right\|_2 , \tag{24}$$

where $\mathbf{\Theta}^v$ is the (unnormalized) dictionary in the vth iteration of this procedure. We then add the wavelet sequence that exhibits the lowest block coherence to the dictionary. We repeat this selection procedure until BM wavelet sequences have been collected. We call the resulting effective sensing matrix "U-NUWS," short for unrestricted NUWS.

While the above procedure does not guarantee the acquisition of M wavelet samples per antenna, we also design a variant that selects exactly M coefficients per antenna, which can simplify NUWS acquisition hardware. The method proceeds as for the U-NUWS dictionary above, but simply limits the selection to M measurements per antenna. We call the resulting effective sensing matrix "R-NUWS," short for restricted NUWS.

As a baseline, we also design a simple multi-antenna sensing matrix that uses the same set of wavelet sequences at all antennas. To this end, we run the above greedy procedure on the overcomplete NUWS matrix $\underline{\mathbf{W}}$ and use that matrix at all antennas. We call the resulting effective sensing matrix "1-NUWS," short for one-antenna NUWS.

IV. RESULTS

We now demonstrate the efficacy of the proposed spatio-spectral whitespace detection approach. We first detail the simulation setup and then present the simulation results.

A. SIMULATION SETUP

We simulate the system depicted in Figure 2 containing multiple single-antenna RF transmitters occupying different frequency bands and communicating with an $B = 8$ antenna receiver equipped with a ULA. We divide the RF spectrum between $2.4\,\text{GHz}$ and $2.5\,\text{GHz}$ into $C = 20$ equally-spaced subbands, each with $Z = 5\,\text{MHz}$ bandwidth. We randomly place the transmitters $1\,\text{m}$ and $280\,\text{m}$ apart of the receiver and randomly set the incident angle of the transmitter in a sector between $10°$ and $135°$. We use the same model and parameters for the receive-side low-noise amplifier (LNA), transmit-side and receive-side mixers, and transmit and receive antennas as in [30]. Concretely, the receiver antenna array is placed at a height of $15\,\text{m}$ with a gain of 10 dBi per antenna. LNA and mixers include nonlinearities of first, third, and fifth order harmonics at $50\,\Omega$ impedance, $-1\,\text{dB}$ gain compression, and a third-order intercept point of $10\,\text{dBm}$. We use Leeson's model [38] with $1\,\text{MHz}$ carrier frequency offset at $-110\,\text{dBc}$ to model the phase noise. We use $8\,\text{dB}$ and $20\,\text{dB}$ respectively, and we set the noise figure to $5\,\text{dB}$ for both the mixer and LNA. We include thermal noise at $290\,\text{K}$ both at the transmitter before the mixer and the receiver before LNA.

For the sake of conciseness, we simulate line-of-sight RF channels with one propagation path and use the path-loss model from [39]. We perform $200\,\text{k}$ Monte-Carlo trials, where we randomize the location, angle, number of transmitting UEs (between $U = 1$ and $U = 5$), spectrum occupancy, and thermal noise. At the receiver side, we measure the RF signal at each of the $B = 8$ antennas by performing NUWS (and other baseline methods) over a duration of $N = 200$ samples. We perform spatio-spectral whitespace detection using LMP with $P = 4$. We also compare our approach to two baselines: (i) Randomly selecting a spatio-spectral block as unused (called "Random") and (ii) performing Nyquist sampling (processing all $N = 200$ samples per antenna) and analyzing the signal power in the beamspace domain (called "Nyquist"). We note that the approach called "Nyquist" uses frequency scanning which first takes a two-dimensional DFT on the multi-antenna RF signal matrix $\mathbf{X}$ followed by calculating the powers of each spatio-spectral block. These powers are then used to declare the whitespace as the block with minimum power. For all whitespace detection methods, we declare an error whenever an algorithm decides that a spatio-spectral resource block was unused but it was, in fact, occupied by a transmitter.

B. SIMULATION RESULTS

Figures 3a, 3b, and 3c show simulation results for $BM = 100$, $BM = 200$, and $BM = 400$ measurements corresponding to subsampling rates of $\eta = 1/16$, $\eta = 1/8$, and $\eta = 1/4$, respectively. We evaluate the empirical error rate versus the average SNR for all active transmitters. We observe that both LMP with U-NUWS and R-NUWS sensing matrices consistently achieve lower error rates than LMP with the same sensing matrix (1-NUWS) for all SNR values. This finding demonstrates that LMP with U-NUWS and R-NUWS can yield lower mutual coherence (and hence better performance) than a näive application of LMP 1-NUWS, which was designed for the single-antenna case [30], to the multi-antenna case. While U-NUWS achieves the lowest error rate among the three dictionaries, the difference between U-NUWS and R-NUWS is relatively small, which implies that R-NUWS is preferrable from an implementation perspective. LMP U-NUWS achieves an error rate of 0.1% for SNR values exceeding $10\,\text{dB}$ with $16\times$ fewer samples than Nyquist sampling. Similarly, at an error rate of 0.1%, LMP with U-NUWS and R-NUWS with a subsampling rate of $\eta = 1/8$ approaches the Nyquist baseline by about $6\,\text{dB}$. Both U-NUWS and R-NUWS enable LMP to achieve an error rate lower than 0.01% with a subsampling rate of $\eta = 1/4$ for SNR values exceeding $5\,\text{dB}$.

We note that an error floor for the subsampling rates $\eta = 1/16$ and $\eta = 1/8$ is visible at high SNR. This observation can be explained by studying the sufficient condition for the success of LMP with $P = 1$ provided in [30, Prop. 1]:

$$\frac{\sum_{j\in\mathcal{U}} \|\mathbf{x}_j\|_2}{\|\mathbf{x}_{\min}\|_2} < \frac{1}{2}\left(\frac{\sigma_{\min}}{\mu_{\mathbf{\Theta}}} + 1\right) - \frac{\|\mathbf{n}\|_2}{\mu_{\mathbf{\Theta}}\|\mathbf{x}_{\min}\|_2}. \qquad (25)$$

Here, $\|\mathbf{x}_{\min}\|_2 = \min_{j\in\mathcal{U}} \|\mathbf{x}_j\|_2$ is the ℓ_2-norm of the block of $\mathbf{x}_i$ that has the minimum ℓ_2-norm among the used blocks indexed by $\mathcal{U}$ and $\sigma_{\min} = \min_{i=1,\dots,B} \sigma_{\mathbf{\Theta}_i}$ is the minimum singular value among all the blocks of $[\mathbf{\Theta}]_i$ with $i = 1,\dots,K$. We see from (25) that the block coherence $\mu_{\mathbf{\Theta}}$ must be minimized and the SNR, which is characterized by the term $\mu_{\mathbf{\Theta}}\|\mathbf{x}_{\min}\|_2/\|\mathbf{n}\|_2$, must be maximized to ensure this condition is met (which guarantees the success of LMP).

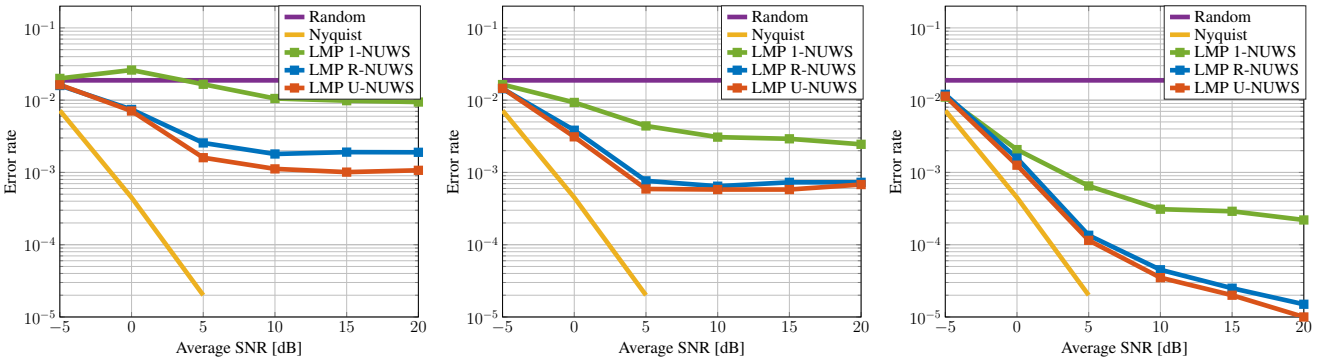

(a) Subsampling rate $\eta = 1/16$ (b) Subsampling rate $\eta = 1/8$ (c) Subsampling rate $\eta = 1/4$

FIGURE 3. Average SNR versus error rate for a multi-antenna spatio-spectral white space detection task. We show the performance for different NUWS sensing matrices and for a random as well as Nyquist-based baseline. We use LMP for (a) $BM = 100$ (subsampling rate $\eta = 1/16$), (b) $BM = 200$ (subsampling rate $\eta = 1/8$), and (c) $BM = 400$ (subsampling rate $\eta = 1/4$) NUWS measurements. At a target error rate of 0.01%, the SNR gap between LMP with U-NUWS and a subsampling rate $\eta = 1/4$ approaches the Nyquist-based baseline by 2 dB.

However, we also see from (25) that even in absence of noise (which is at infinite SNR), the block coherence limits the performance of LMP. Hence, to further improve the performance at high SNR, one must design sampling matrices with lower block coherence, which is fundamentally limited by the Welch lower bound [40] and can be reduced by increasing the number of compressive measurements (which would increase the subsampling rates and degrade sampling efficiency).

V. CONCLUSIONS

We have proposed a novel spatio-spectral whitespace detection pipeline for multi-antenna RF transceivers. Our method first acquires NUWS measurements at multiple antennas and then uses LMP to identify unused resources in both the angular and frequency domains. We have shown that properly-designed multi-antenna NUWS sensing matrices yield lower mutual coherence, which manifests itself in lower error rates. Simulation results have demonstrated that LMP-based spatio-spectral whitespace detection can approach the performance of Nyquist sampling by about 2 dB SNR at a target error rate of only 0.01% with a subsampling rate of $\eta = 1/4$.

There are many avenues for future work. An in-depth study of the impact of more hardware impairments (such as carrier frequency offsets and symbol timing mismatches) on our framework would be interesting. The development of a hardware prototype that performs multi-antenna NUWS for energy-efficient spatio-spectral whitespace detection is an ongoing work. Investigating the efficacy of spectral reallocation of UEs using our pipeline is an interesting open problem. The development of algorithms for on-device spatio-spectral whitespace detection from compressive measurements that require lower complexity than LMP is a challenging research topic.

.

APPENDIX A PROOF OF PROPOSITION 1

In what follows, we assume equally sized blocks $N_i = N/K$ and normalization $[\hat{\mathbf{W}}_b]_k^H [\hat{\mathbf{W}}_b]_k = \mathbf{I}_{N_i}$ of the frequency-domain (FD) beamspace NUWS matrices $\hat{\mathbf{W}}_b = \mathbf{W}_b \mathbf{F}_N^H$, $b = 1, \ldots, B$. We start by explicitly stating the effective sensing matrix:

$$\boldsymbol{\Theta} = \begin{bmatrix} [\mathbf{F}_B^H]_{1,1}\hat{\mathbf{W}}_1 & \cdots & [\mathbf{F}_B^H]_{1,B}\hat{\mathbf{W}}_1 \\ [\mathbf{F}_B^H]_{2,1}\hat{\mathbf{W}}_2 & \cdots & [\mathbf{F}_B^H]_{2,B}\hat{\mathbf{W}}_2 \\ \vdots & \ddots & \vdots \\ [\mathbf{F}_B^H]_{B,1}\hat{\mathbf{W}}_B & \cdots & [\mathbf{F}_B^H]_{B,B}\hat{\mathbf{W}}_B \end{bmatrix}. \tag{26}$$

The definition of the block coherence in (21) relies on the following spectral norms:

$$\|[\boldsymbol{\Theta}]_i^H [\boldsymbol{\Theta}]_{i'}\|_2 = \left\| \sum_{b=1}^{B} [\mathbf{F}_B]_{b,q} [\hat{\mathbf{W}}_b]_k^H [\hat{\mathbf{W}}_b]_{k'} [\mathbf{F}_B^H]_{b,q'} \right\|_2. \tag{27}$$

Here, (i, i') are the block indices in the effective sensing matrix $\boldsymbol{\Theta}$, (k, k') are the block indices in the FD-NUWS matrices $\hat{\mathbf{W}}_b$ (corresponding to blocks of N_i adjacent frequencies), and (q, q') are the antenna indices. We have the mappings $i = k + (q-1)K$ and $i' = k' + (q'-1)K$ between blocks of the effective sensing matrix $\boldsymbol{\Theta}$ and blocks in the FD-NUWS matrices $\hat{\mathbf{W}}_q$, $q = 1, \ldots, B$, where $K = N/N_i$ is the number of blocks per $\hat{\mathbf{W}}_q$ matrix and N_i is the block size (corresponding to N_i adjacent frequencies). For example, the submatrix $[\hat{\mathbf{W}}_q]_k \in \mathbb{C}^{M \times N_i}$ refers to the kth block in the qth FD-NUWS matrix $\hat{\mathbf{W}}_b$ and is equal to $[\boldsymbol{\Theta}]_i$ with the mapping $i = k + (q-1)K$. In order to obtain a bound on the block coherence in (27), we have to analyze the following three cases:

Case 1 ($k = k'$ and $q \neq q'$)

We start by using the assumption that the columns of the individual blocks of the FD-NUWS matrices $\hat{\mathbf{W}}_b$ are unitary,

i.e., $[\hat{\mathbf{W}}_b]_k^H[\hat{\mathbf{W}}_b]_k = \mathbf{I}_{N_i}$. With this assumption, the right-hand side (RHS) of (27) simplifies to

$$\|[\mathbf{\Theta}]_i^H[\mathbf{\Theta}]_{i'}\|_2 = \left\|\sum_{b=1}^{B}[\mathbf{F}_B]_{b,q}\mathbf{I}_{N_i}[\mathbf{F}_B^H]_{b,q'}\right\|_2. \tag{28}$$

Since $\sum_{b=1}^{B}[\mathbf{F}_B]_{b,q}[\mathbf{F}_B^H]_{b,q'} = 0$ for $q \neq q'$, a consequence of the unitarity of the DFT matrix, we have $\|[\mathbf{\Theta}]_i^H[\mathbf{\Theta}]_{i'}\|_2 = 0$.

Case 2 ($k \neq k'$ and $q = q'$)

Since $q = q'$, we have that $[\mathbf{F}_B]_{b,q}[\mathbf{F}_B^H]_{b,q'} = 1/B$; a consequence of the unitarity of the DFT matrix. With this, the spectral norm in (27) can be written as

$$\|[\mathbf{\Theta}]_i^H[\mathbf{\Theta}]_{i'}\|_2 = \frac{1}{B}\left\|\sum_{b=1}^{B}[\hat{\mathbf{W}}_b]_k^H[\hat{\mathbf{W}}_b]_{k'}\right\|_2. \tag{29}$$

While the RHS could be calculated exactly for a given dictionary, we now bound this expression by the block coherence $\mu_{\hat{\mathbf{W}}_b}$ of each FD-NUWS submatrix $\hat{\mathbf{W}}_b$, $b = 1, \ldots, B$, using the triangle inequality:

$$\frac{1}{B}\sum_{b=1}^{B}\left\|[\hat{\mathbf{W}}_b]_k^H[\hat{\mathbf{W}}_b]_{k'}\right\|_2 \leq \frac{1}{B}\sum_{b=1}^{B}\mu_{\hat{\mathbf{W}}_b}. \tag{30}$$

Case 3 ($k \neq k'$ and $q \neq q'$)

For this case, we directly apply the triangle inequality to the RHS of (27), which yields

$$\begin{aligned}\|[\mathbf{\Theta}]_i^H[\mathbf{\Theta}]_{i'}\|_2 &\leq \sum_{b=1}^{B}\left\|[\mathbf{F}_B]_{b,q}[\hat{\mathbf{W}}_b]_k^H[\hat{\mathbf{W}}_b]_{k'}[\mathbf{F}_B^H]_{b,q'}\right\|_2 \\ &\overset{(a)}{=} \frac{1}{B}\sum_{b=1}^{B}\left\|[\hat{\mathbf{W}}_b]_k^H[\hat{\mathbf{W}}_b]_{k'}\right\|_2 \overset{(b)}{\leq} \frac{1}{B}\sum_{b=1}^{B}\mu_{\hat{\mathbf{W}}_b}.\end{aligned} \tag{31}$$

Here, (a) follows from the unitarity of the DFT matrix and (b) uses the definition of the block coherence $\mu_{\hat{\mathbf{W}}_b}$ of each FD-NUWS submatrix $\hat{\mathbf{W}}_b$.

By combining (28), (29), and (31), we obtain the bound in (22), which concludes the proof.

APPENDIX B PROOF OF PROPOSITION 2

We follow the steps of the proof of Appendix A but exploit the fact that all B NUWS matrices $\mathbf{W}_b$ are the same, i.e., $\hat{\mathbf{W}}_1 = \hat{\mathbf{W}}_b$ for all $b = 1, \ldots, B$. Case 1 ($k = k'$ and $q \neq q'$) remains the same. Case 2 ($k \neq k'$ and $q = q'$) leads to

$$\|[\mathbf{\Theta}]_i^H[\mathbf{\Theta}]_{i'}\|_2 = \frac{1}{B}\left\|\sum_{b=1}^{B}[\hat{\mathbf{W}}_1]_k^H[\hat{\mathbf{W}}_1]_{k'}\right\|_2 \tag{32}$$

$$= \left\|[\hat{\mathbf{W}}_1]_k^H[\hat{\mathbf{W}}_1]_{k'}\right\|_2. \tag{33}$$

Case 3 ($k \neq k'$ and $q \neq q'$) results in

$$\|[\mathbf{\Theta}]_i^H[\mathbf{\Theta}]_{i'}\|_2 = \left\|[\hat{\mathbf{W}}_1]_k^H[\hat{\mathbf{W}}_1]_{k'}\sum_{b=1}^{B}[\mathbf{F}_B]_{b,q}[\mathbf{F}_B^H]_{b,q'}\right\|_2 = 0, \tag{34}$$

because the DFT matrix is unitary. Since, (33) holds with equality, we have that $\mu_{\mathbf{\Theta}} = \mu_{\hat{\mathbf{W}}_1}$, which concludes the proof.

REFERENCES

[1] "Cisco visual networking index: Global mobile data traffic forecast update, 2015-2020 white paper," http://www.cisco.com/c/en/us/solutions/collateral/service-provider/visual-networking-index-vni/white_paper_c11-520862.html, Feb. 2016.
[2] T. L. Marzetta, "Noncooperative cellular wireless with unlimited numbers of base station antennas," *IEEE Trans. Wireless Commun.*, vol. 9, no. 11, pp. 3590–3600, Nov. 2010.
[3] J. Hoydis, S. ten Brink, and M. Debbah, "Massive MIMO: How many antennas do we need?" in *Proceedings of the 49th Annual Allerton Conference on Communication, Control, and Computing*, Sept. 2011, pp. 545–550.
[4] H. Q. Ngo, E. G. Larsson, and T. L. Marzetta, "Energy and spectral efficiency of very large multiuser MIMO systems," *IEEE Trans. Commun.*, vol. 61, no. 4, pp. 1436 – 1449, Apr. 2013.
[5] E. Björnson, J. Hoydis, M. Kountouris, and M. Debbah, "Massive MIMO systems with non-ideal hardware: Energy efficiency, estimation, and capacity limits," *IEEE Trans. Inf. Theory*, vol. 60, no. 11, pp. 7112–7139, Sept. 2014.
[6] S. Haykin, D. J. Thomson, and J. H. Reed, "Spectrum sensing for cognitive radio," *Proc. IEEE*, vol. 97, no. 5, pp. 849–877, May 2009.
[7] H. Sun, A. Nallanathan, C.-X. Wang, and Y. Chen, "Wideband spectrum sensing for cognitive radio networks: A survey," *IEEE Wireless Commun.*, vol. 20, no. 2, pp. 74–81, Apr. 2013.
[8] D. L. Donoho, "Compressed sensing," *IEEE Trans. Inf. Theory*, vol. 52, no. 4, pp. 1289–1306, Apr. 2006.
[9] E. J. Candès and M. B. Wakin, "An introduction to compressive sampling," *IEEE Signal Process. Mag*, vol. 25, no. 2, pp. 21–30, Mar. 2008.
[10] T.-H. Yu, O. Sekkat, S. Rodriguez-Parera, D. Markovic, and D. Cabric, "A wideband spectrum-sensing processor with adaptive detection threshold and sensing time," *IEEE Trans. Circuits Syst. I, Reg. Papers*, vol. 58, no. 11, pp. 2765–2775, Nov. 2011.
[11] Z. Tian and G. B. Giannakis, "Compressed sensing for wideband cognitive radios," in *IEEE Intl. Conf. on Acoustics, Speech and Signal Processing (ICASSP)*, vol. 4, Apr. 2007, pp. 1357–1360.
[12] Y. L. Polo, Y. Wang, A. Pandharipande, and G. Leus, "Compressive wide-band spectrum sensing," in *IEEE Intl. Conf. on Acoustics, Speech and Signal Processing (ICASSP)*, Apr. 2009, pp. 2337–2340.
[13] M. Wakin, S. Becker, E. Nakamura, M. Grant, E. Sovero, D. Ching, J. Yoo, J. Romberg, A. Emami-Neyestanak, and E. Candes, "A nonuniform sampler for wideband spectrally-sparse environments," *IEEE J. Emerg. Sel. Topics Circuits Syst.*, vol. 2, no. 3, pp. 516–529, Sept. 2012.
[14] B. Hamdaoui, B. Khalfi, and M. Guizani, "Compressed wideband spectrum sensing: Concept, challenges, and enablers," *IEEE Commun. Mag.*, vol. 56, no. 4, pp. 136–141, Apr. 2018.
[15] X. Zhang, Y. Ma, Y. Gao, and S. Cui, "Real-time adaptively regularized compressive sensing in cognitive radio networks," *IEEE Trans. Veh. Technol.*, vol. 67, no. 2, pp. 1146–1157, Sep. 2018.
[16] H. Qi, X. Zhang, and Y. Gao, "Subspace-aided low-complexity blind compressive spectrum sensing over TV whitespace," in *IEEE Global Commun. Conf.*, Dec. 2018, pp. 1–6.
[17] P. Chen, Z. Cao, Z. Chen, L. Liu, and M. Feng, "Compressed sensing-based DOA estimation with unknown mutual coupling effect," *Electronics*, vol. 7, no. 12, Dec. 2018.
[18] D. E. Bellasi, L. Bettini, C. Benkeser, T. Burger, Q. Huang, and C. Studer, "VLSI design of a monolithic compressive-sensing wideband analog-to-information converter," *IEEE J. Emerg. Sel. Topics Circuits Syst.*, vol. 3, no. 4, pp. 552–565, Dec. 2013.
[19] T. Haque, R. T. Yazicigil, K. J.-L. Pan, J. Wright, and P. R. Kinget, "Theory and design of a quadrature analog-to-information converter for energy-efficient wideband spectrum sensing," *IEEE Trans. Circuits Syst. I*, vol. 62, no. 2, pp. 527–535, Oct. 2015.
[20] R. T. Yazicigil, T. Haque, J. Wright, and P. R. Kinget, "Band-pass compressive sampling as an enabling technology for rapid wideband rf spectrum sensing," in *Proc. Asilomar Conf. Signals, Syst., Comput.*, Nov. 2016, pp. 1032–1036.
[21] W. Liu, Z. Huang, X. Wang, and W. Sun, "Design of a single channel modulated wideband converter for wideband spectrum sensing: Theory, architecture and hardware implementation," *Sensors*, vol. 17, no. 5, May 2017.
[22] R. T. Yazicigil, T. Haque, P. R. Kinget, and J. Wright, "Taking compressive sensing to the hardware level: Breaking fundamental radio-frequency hardware performance tradeoffs," *IEEE Signal Process. Mag.*, vol. 36, no. 2, pp. 81–100, Feb. 2019.

[23] M. A. Davenport, J. N. Laska, J. R. Treichler, and R. G. Baraniuk, "The pros and cons of compressive sensing for wideband signal acquisition: Noise folding versus dynamic range," *IEEE Trans. Signal Process.*, vol. 60, no. 9, pp. 4628–4642, Sep. 2012.
[24] M. Pelissier and C. Studer, "Non-uniform wavelet sampling for RF analog-to-information conversion," *IEEE Trans. Circuits Syst. I, Reg. Papers*, Aug. 2017.
[25] P. Maechler, D. E. Bellasi, A. Burg, N. Felber, H. Kaeslin, and C. Studer, "Sparsity-based real-time audio restoration," in *Proc. Conference on Design & Architectures for Signal & Image Processing (DASIP)*, Oct. 2012.
[26] P. Maechler, C. Studer, D. E. Bellasi, A. Maleki, A. Burg, N. Felber, H. Kaeslin, and R. G. Baraniuk, "VLSI design of approximate message passing for signal restoration and compressive sensing," *IEEE J. Emerg. Sel. Topics Circuits Syst.*, vol. 2, no. 3, pp. 579–590, Sept. 2012.
[27] F. Chen, A. P. Chandrakasan, and V. M. Stojanovic, "Design and analysis of a hardware-efficient compressed sensing architecture for data compression in wireless sensors," *IEEE J. Solid-State Circuits*, vol. 47, no. 3, pp. 744–756, Feb. 2012.
[28] F. Ren and D. Marković, "18.5 a configurable 12-to-237KS/s 12.8 mW sparse-approximation engine for mobile ExG data aggregation," in *IEEE Int. Solid-State Circuits Conf.*, Feb. 2015.
[29] J. Yoo, Y. Xie, A. Harms, W. U. Bajwa, and R. Calderbank, "Finding zeros: Greedy detection of holes," *ArXiv preprint: 1303.2048*, Mar. 2013.
[30] E. Gönültaş, M. Taghavi, S. Soni, A. B. Apsel, and C. Studer, "Identifying unused RF channels using least matching pursuit," in *Proc. IEEE 21st Int. W. Signal Process. Advances Wireless Commun.*, May 2020, pp. 1–5.
[31] A. Goldsmith, *Wireless communications*. Cambridge University Press, 2005.
[32] D. Tse and P. Viswanath, *Fundamentals of wireless communication*. Cambridge University Press, 2005.
[33] L. Godara, "Application of antenna arrays to mobile communications. II. beam-forming and direction-of-arrival considerations," *Proc. IEEE*, vol. 85, no. 8, pp. 1195–1245, Aug. 1997.
[34] A. Sayeed and J. Brady, "Beamspace MIMO for high-dimensional multiuser communication at millimeter-wave frequencies," in *IEEE Global Communications Conference (GLOBECOM)*, Dec. 2013, pp. 3679–3684.
[35] Y. C. Eldar, P. Kuppinger, and H. Bolcskei, "Block-sparse signals: Uncertainty relations and efficient recovery," *IEEE Trans. Signal Process.*, vol. 58, no. 6, pp. 3042–3054, Jun. 2010.
[36] M. Pelissier, G. Masson, L. Ouvry, L. F. F. Dias, and M. Marnat, "Hardware platform of analog-to-information converter using non uniform wavelet bandpass sampling for RF signal activity detection," in *Proc. IEEE Int. Symp. Circuits Syst.*, May 2018.
[37] X. Liu, E. Gönültaş, and C. Studer, "Analog-to-Feature (A2F) conversion for Audio-Event classification," in *Proc. 26th European Signal Process. Conf.*, Roma, Italy, Sep. 2018, pp. 2275–2279.
[38] D. B. Leeson, "A simple model of feedback oscillator noise spectrum," *Proc. IEEE*, vol. 54, no. 2, pp. 329–330, Feb. 1966.
[39] A. Tang, J. Sun, and K. Gong, "Mobile propagation loss with a low base station antenna for NLOS street microcells in urban area," in *Proc. IEEE Veh. Technol. Conf*, May 2001, pp. 333–336.
[40] L. Welch, "Lower bounds on the maximum cross correlation of signals," *IEEE Trans. Inf. Theory*, vol. 20, no. 3, pp. 397–399, May 1974.

EMRE GÖNÜLTAŞ received the B.S. degree in Electrical and Electronics Engineering from KTO Karatay University, Turkey, in 2014. During his undergraduate studies, he was involved in wireless communications and biomedical signal processing research projects. Emre started his Ph.D. work in School of Electrical and Computer Engineering at Cornell University in 2016, and received the M.S. degree in Electrical and Computer Engineering from Cornell University, Ithaca, NY, in 2018. His Ph.D. work includes algorithm development for hardware-aware machine learning, feature extraction, compressed spectrum sensing, and wireless communications. During the first year of his Ph.D., Emre was a finalist of the Qualcomm Innovation Fellowship. Emre also held two summer internships in localization and sensing at Nokia Bell Labs and received the Bell Labs Outstanding Summer Intern award in 2020. After completion of his Ph.D. degree, Emre started a position as a baseband system developer at Ericsson.

SWETA SONI received the B.Tech. degree in electrical engineering from the Indian Institute of Technology, Delhi in 2018, and is currently pursuing Ph.D. degree in Electrical and Computer Engineering from Cornell University, Ithaca, NY. Her current research interests include RF, analog, and mixed-signal circuit design focusing on wideband software-defined radios and spectrum sensing.

ALYSSA B. APSEL received the B.S. from Swarthmore College in 1995 and the Ph.D. from Johns Hopkins University, Baltimore, MD, in 2002. She joined Cornell University in 2002, where she is currently Director of Electrical and Computer Engineering. The focus of her research is on power-aware mixed signal circuits and design for highly scaled CMOS and modern electronic systems. Her current research is on the leading edge of ultra-low power and flexible RF interfaces for IoT. Her group has pioneered the use of coupled oscillators for network synchronization of mesh networks. She has authored or coauthored over 100 refereed publications including one book in related fields of RF mixed signal circuit design, ultra-low power radio, interconnect design and planning, photonic integration, and process invariant circuit design techniques resulting in ten patents. She has received a number of best paper awards and the National Science Foundation CAREER Award in addition to being selected by Technology Review Magazine as one of the Top Young Innovators in 2004. More recently Professor Apsel served as a Distinguished Lecturer for IEEE CAS from 2018-2019 and was named an IEEE Fellow.

CHRISTOPH STUDER (S'06, M'10, SM'14) is an Associate Professor at the Department of Information Technology and Electrical Engineering at ETH Zürich, Zürich, Switzerland. In 2009, he received a Ph.D. degree in Electrical Engineering from ETH Zürich. In 2005, he was a Visiting Researcher with the Smart Antennas Research Group at Stanford University. From 2006 to 2009, he was a Research Assistant in both the Integrated Systems Laboratory and the Communication Technology Laboratory (CTL) at ETH Zürich. From 2009 to 2012, Dr. Studer was a Postdoctoral Researcher at CTL, ETH Zürich, and the Digital Signal Processing Group at Rice University, Houston, TX. In 2013, he has held the position of Research Scientist at Rice University. From 2014 to 2019, Dr. Studer was an Assistant Professor at Cornell University, Ithaca, NY. From 2019 to 2020, he was an Associate Professor at Cornell University and at Cornell Tech in New York City. In 2020, he joined ETH Zürich, and since 2014, he has been an Adjunct Professor at Rice University.

Dr. Studer's research interests include the design of application-specific integrated circuits, as well as wireless communications, digital signal processing, optimization, and machine learning.

Dr. Studer received ETH Medals for his M.S. and Ph.D. theses in 2006 and 2009, respectively. He received a Swiss National Science Foundation fellowship for Advanced Researchers in 2011 and a US National Science Foundation CAREER Award in 2017. Dr. Studer won a Michael Tien '72 Excellence in Teaching Award from the College of Engineering, Cornell University, in 2016. He shared the Swisscom/ICTnet Innovations Award in both 2010 and 2013. Dr. Studer was the winner of the Student Paper Contest of the 2007 Asilomar Conf. on Signals, Systems, and Computers, received a Best Student Paper Award of the 2008 IEEE Int. Symp. on Circuits and Systems (ISCAS), and shared the best Live Demonstration Award at the IEEE ISCAS in 2013. Dr. Studer is currently an Associate Editor for the IEEE Open Journal of Circuits and Systems (OJ-CAS) and the IEEE Communications Letters. In 2019, he was the Technical Program Chair of the Asilomar Conference on Signals, Systems, and Computers, and a Technical Program Co-Chair of the IEEE International Workshop on Signal Processing Systems (SiPS).